

## Perspective

# Solid electrolyte interphases in lithium metal batteries

Ben Jagger<sup>1</sup> and Mauro Pasta<sup>1,2,\*</sup>

## SUMMARY

**Lithium metal batteries (LMBs) have recently received enormous interest as a higher energy density alternative to conventional lithium-ion batteries (LIBs). However, the commercialization of LMBs is currently impeded by poor cycle life due to inhomogeneous lithium deposition and active lithium loss. These are controlled by the solid electrolyte interphase (SEI) that forms on the anode surface, and there have been numerous reported strategies to produce SEIs with desired properties. However, these have not been sufficient to achieve the high cycling stabilities necessary for widespread LMB commercialization, requiring additional understanding of the SEI. In this perspective, we highlight recent progress in characterizing the SEI that forms in LMBs and outline the need to consider SEI nanostructure, transport, and mechanical properties together. We conclude by prescribing several key research fronts necessary for an accurate, systematic study of the SEI that will guide future electrolyte design and enable the development of safe and stable LMBs.**

## INTRODUCTION

Lithium metal batteries (LMBs), with lithium metal as the anode, have recently received enormous interest as a higher energy density alternative to conventional lithium-ion batteries (LIBs) for high-end electric vehicles<sup>1</sup> and novel applications including electric flight.<sup>2</sup> However, successful LMB commercialization will demand batteries with high specific energies (above 500 Wh kg<sup>-1</sup>) at low cost (below US\$100 kWh<sup>-1</sup>).<sup>3</sup> Batteries must also retain 80%–90% of their capacity over 1,000 cycles, requiring a coulombic efficiency (CE) of over 99.99% in zero-excess-lithium cells.<sup>4,5</sup> Achieving these targets additionally requires the implementation of high-energy cathodes and the development of novel electrolytes compatible with both electrodes. Liquid electrolytes are ideal as they ensure good electrode contact<sup>6</sup> and they are compatible with existing manufacturing routes established for LIBs.<sup>1</sup>

However, lithium metal anodes operate outside of the electrochemical stability window of any electrolyte, and spontaneous reduction of electrolyte species occurs when the anode potential is reduced below the potential of electrolyte reduction.<sup>7</sup> Kinetic stability is afforded by the formation of a surface layer composed of the insoluble reaction products,<sup>8</sup> which was first named the solid electrolyte interphase (SEI) by Peled in 1979.<sup>9</sup>

LMB cycle life is currently limited by inhomogeneous lithium plating/stripping, which exposes additional lithium to the electrolyte and results in active lithium loss due to the formation of SEI and electrochemically isolated “dead” lithium.<sup>10</sup> This lowers the CE; hence, excess lithium in the form of lithium foil is currently needed to extend

## CONTEXT & SCALE

Lithium metal batteries (LMBs) are a promising alternative to lithium-ion batteries (LIBs) owing to the high theoretical specific capacity (3,860 mAh g<sup>-1</sup>) and low electrode potential (−3.04 V vs. standard hydrogen electrode) of lithium metal. High-specific-energy LMBs would enable novel high-energy applications, such as electric flight, and facilitate the electrification necessary to meet net-zero targets. However, the commercialization of LMBs is currently limited by their poor cycle life.

Reactions between the anode and electrolyte form a thin solid electrolyte interphase (SEI) layer that regulates lithium plating/stripping morphology and controls LMB cycling stability, which has been the focus of numerous research efforts. In this perspective, we highlight recent breakthroughs and common misconceptions in the literature and identify several key research fronts necessary for accurate SEI characterization, with emphasis on its nanostructure, transport, and mechanical properties.

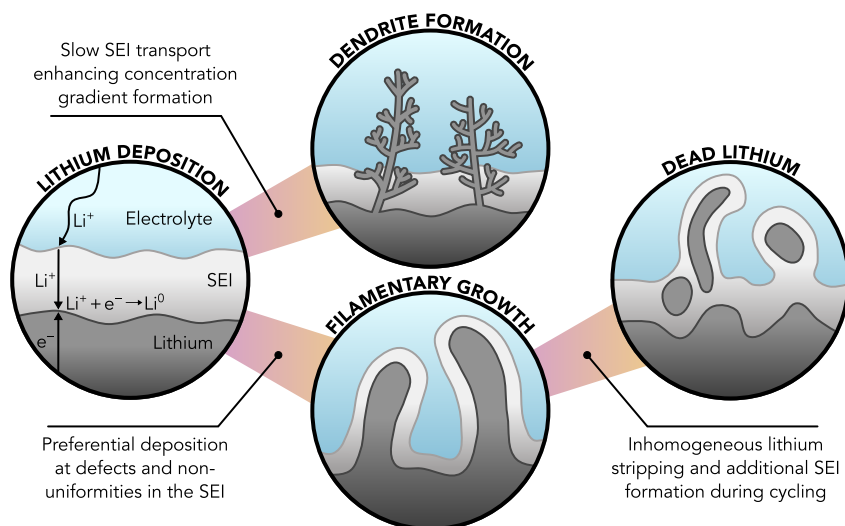


**Figure 1. Influence of the solid electrolyte interphase on lithium deposition morphology**

Schematics of the formation of dendrites, lithium filaments, and dead lithium. The solid electrolyte interphase (SEI) can enhance  $\text{Li}^+$  concentration gradients, causing dendrite formation before the bulk electrolyte diffusion limitation and causing cell failure.<sup>23</sup> Preferential lithium deposition can also occur at weak points or defects in the SEI, resulting in non-uniform filamentary growth. Lithium filaments can grow and interweave into a high-surface-area mossy morphology.<sup>22</sup> Inhomogeneous stripping and additional SEI formation during cycling can leave electrochemically isolated dead lithium.<sup>10</sup>

cycle life to practical values,<sup>11</sup> reducing the specific energy. The CE of the lithium metal anode (determined from  $\text{Cu}|\text{Li}$  half cells, for example, as described by Hobold et al.<sup>4</sup>) is therefore a useful metric for assessing cell stability. This non-uniform lithium plating and stripping behavior is influenced by the fundamental properties of the liquid electrolyte and metallic lithium. Electrolyte transport and thermodynamic properties govern the development of salt concentration gradients and overpotentials during cell operation.<sup>12,13</sup> In extreme cases, the electrolyte can be completely depleted of salt at the anode surface during charge, leading to the nucleation of fractal, tip-growing lithium dendrites, and their associated safety concerns.<sup>14,15</sup> Electrolyte charge-transfer kinetics has also recently been demonstrated to influence deposition morphology, with fast interfacial charge-transfer observed to positively correlate with CE.<sup>16</sup> Additionally, the microstructure and anisotropic nanomechanical properties of lithium metal<sup>17,18</sup> impact the cycling behavior, with inhomogeneous stripping observed to be influenced by crystallographic texture,<sup>19</sup> and more uniform deposition morphologies achieved under applied stack pressures both above<sup>20</sup> and below<sup>21</sup> the macroscopic yield stress.

However, the degradation phenomena observed in LMBs cannot be fully described by the properties of lithium and the electrolyte alone,<sup>22,23</sup> and ultimately, it is the SEI that controls cycling performance by regulating lithium morphology and dead lithium formation.<sup>24</sup> This is represented schematically in Figure 1, which shows how the SEI can lead to early dendrite initiation, and how it can promote filamentary growth and the subsequent formation of dead lithium. The SEI needs to be electrically insulating, ionically conductive, and mechanically robust to effectively passivate the lithium anode,<sup>25</sup> and it has been widely thought that the SEI should be rich in inorganic components,<sup>26</sup> with a positive correlation observed between  $\text{LiF}$ -content and cycling performance.<sup>27</sup> This has led to the development of numerous strategies to produce SEIs with desired compositions through design of

<sup>1</sup>Department of Materials, University of Oxford, Oxford OX1 3PH, UK

<sup>2</sup>The Faraday Institution, Quad One, Didcot OX11 0RA, UK

\*Correspondence:  
mauro.pasta@materials.ox.ac.uk  
<https://doi.org/10.1016/j.joule.2023.08.007>

advanced electrolytes with controlled chemistries and solvation structures.<sup>1,28–36</sup> Artificial SEIs have also been implemented to promote stable LMB cycling,<sup>37,38</sup> although these are unable to self-repair. However, these strategies have not been sufficient to achieve the high cycling stabilities required for LMB commercialization. Fang et al. and Hobold and Gallant have demonstrated that electrolyte systems with CEs above 95% result in limited dead lithium formation during cycling<sup>10,39</sup>; hence, additional losses due to continuous SEI formation must be reduced for further improvement. This will require a better understanding of the properties of the SEI and their influence on cycling performance, enabling the rational design of SEIs to guide future electrolyte development.

## SEI PROPERTIES

### Nanostructure

A complete understanding of the SEI first requires an accurate characterization of its structure and composition. One of the most popular structural models of SEI is the mosaic model (Figure 2A), first proposed by Peled et al. in 1997.<sup>40</sup> It is assumed that multiple SEI components form simultaneously, producing a heterogeneous “mosaic of microphases.” The driving force for reduction is greatest at the anode surface, producing an inner SEI layer composed of inorganic, fully reduced salt decomposition products. This shields the remaining electrolyte; hence, the outer layer is composed of more organic, partially reduced phases from solvent decomposition. Recent evidence additionally suggests that this outer organic layer is porous and permits electrolyte impregnation,<sup>41,42</sup> potentially facilitating desolvation.<sup>43</sup> A summary of typical liquid electrolyte solvents, salts, and additives used in LMB research, and their main reduction products is provided in Table S1.

The recent utilization of cryogenic transmission electron microscopy (cryo-TEM) techniques has enabled direct imaging of the SEI with reduced beam damage.<sup>44</sup> In some electrolyte systems, the observed SEI structures are in agreement with the mosaic model and generally consist of small crystalline domains of  $\text{Li}_2\text{O}$  and  $\text{Li}_2\text{CO}_3$  in an amorphous organic matrix, with a total thickness on the order of tens of nanometers (Figure 2B).<sup>21,44</sup> However, this is not always the case, and the SEI has been reported to be completely amorphous (Figure 2C)<sup>45,46</sup> or to form with a multilayered structure (Figure 2B).<sup>44,47</sup> The structure can significantly impact cycling performance, with a heterogeneous mosaic SEI observed to lead to non-uniform stripping, which is prevented by a multilayered SEI.<sup>24</sup> Cryo-TEM alone can only identify crystalline SEI components, requiring additional spectroscopic tools like energy dispersive X-ray spectroscopy (EDX),<sup>45</sup> X-ray photoelectron spectroscopy (XPS),<sup>46</sup> or electron energy loss spectroscopy (EELS)<sup>47</sup> to determine the nature of amorphous components, revealing that they can be either organic or inorganic. Han et al. have also reported an amorphous lithium transition layer between the SEI and bulk lithium, believed to be generated by the doping of lithium with elements from electrolyte decomposition during electrodeposition.<sup>47,49</sup> This complicates the measurement of SEI thickness.

Additionally, the observed SEI thickness depends on how the sample is prepared. Zhang et al. adapted a thin film vitrification method to preserve the solid-liquid interface and found that the SEI swells in contact with electrolyte, resulting in thicknesses as much as twice as large as in the dry state. For example, 1 M lithium bis(fluorosulfonyl)imide (LiFSI) in 1,2-dimethoxyethane (DME) resulted in SEI thicknesses of approximately 17.5 and 10 nm in the vitrified and dry states, respectively.<sup>50</sup> This is indicative of a porous SEI, and a negative correlation was observed between

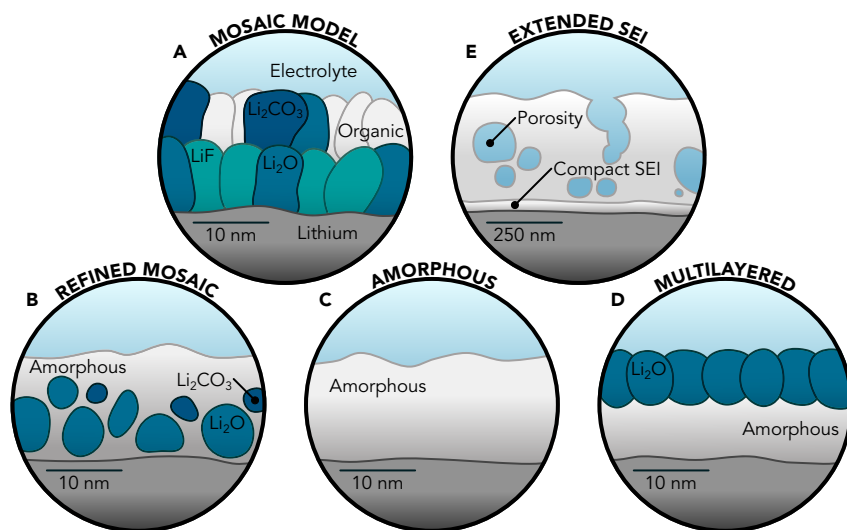


**Figure 2. Solid electrolyte interphase nanostructure**

(A) The traditional mosaic model of the solid electrolyte interphase (SEI).<sup>40</sup> The SEI is predominantly inorganic close to the lithium anode and becomes more organic toward the electrolyte.  
 (B) Schematic representation of typical heterogeneous mosaic SEI structures.<sup>21,44</sup>  
 (C) Schematic representation of typical amorphous SEI structures.<sup>45,46</sup>  
 (D) Schematic representation of typical multilayered SEI structures.<sup>44,47</sup>  
 (E) Schematic representation of an extended SEI. A porous extended SEI layer can form on the lithium surface and can be removed during sample preparation steps, leaving only the compact SEI.<sup>48</sup>

swelling ratio and CE, suggesting that excessive porosity may be detrimental to cell performance.<sup>50</sup> Zachman et al. also examined the structures formed at the solid-liquid interfaces in LMBs and observed lithium metal filaments surrounded by a porous, organic extended SEI of around 500 nm thickness, which is likely to be removed during typical sample washing steps, leaving behind just the compact SEI described previously (Figure 2E).<sup>48</sup> Such an extended SEI has also been observed by *in situ* liquid cell TEM,<sup>27</sup> and its presence suggests that more active lithium is lost during SEI formation than previously believed. It is therefore important to ensure that any sample preparation steps do not significantly alter the sample and that SEI imaging and analysis are performed under operating conditions when possible. The majority of reported SEI characterization is performed *ex situ* and may not be representative of the true state of the SEI.

### Composition

The chemical composition of the SEI is typically determined using XPS.<sup>51</sup> In fact, XPS results lead to the original mosaic model<sup>40</sup> and have prompted the exploration of highly fluorinated electrolytes due to the belief that LiF is a crucial component in the SEI.<sup>52</sup> However, XPS measurements must be performed with care, as results have been demonstrated to vary with sample preparation method, and the surface chemistry can change over time even under the ultrahigh vacuum (UHV) in the analysis chamber.<sup>51</sup> Yu et al. also recently showed that several common salts decompose to form LiF during the Ar<sup>+</sup> sputtering often used for depth profiling.<sup>53</sup> Combining this with the low lateral resolution of XPS and the difficulties in accurately determining a composition from relative peak intensities,<sup>54</sup> any SEI structures determined solely with XPS should be treated as rough estimates, and additional techniques are required for verification. The development of novel *in situ* and *operando* techniques

would also be incredibly valuable to probe the processes occurring at the solid-liquid interface under realistic operating conditions.<sup>55,56</sup>

Despite the belief that LiF is a major SEI component, it has rarely been observed in the compact SEI using cryo-TEM or high-resolution spectroscopy. Huang et al. instead found that the fluorine from electrolyte decomposition exists as LiF particles with a diameter of up to 400 nm, randomly distributed over the anode surface.<sup>57</sup> LiF particles were also observed in other studies,<sup>58,59</sup> further suggesting that LiF in the SEI cannot solely be responsible for improved cycling performance observed in highly fluorinated electrolytes.<sup>4</sup> The benefits of highly fluorinated electrolytes could therefore be 2-fold: (1) Fluorine is highly electronegative, and its presence raises the potential of electrolyte reduction of fluorinated species relative to their non-fluorinated counterparts. This increases the driving force for electrolyte reduction,<sup>34,52</sup> enhancing the kinetics of SEI formation and potentially allowing fast SEI repair.<sup>60</sup> Oxidative stability is also increased, enabling improved performance with high-voltage cathodes. (2) Fluorinated solvents are typically weakly solvating, leading to significant ion-ion interactions that increase the activity of Li<sup>+</sup> in the electrolyte, increasing the electrode potential.<sup>61,62</sup> This weakens the reducing ability of the electrode, increases the rate of charge transfer, and increases the lithium surface energy, promoting low-surface-area deposition and an anion-derived SEI.<sup>16,61,62</sup>

Additional techniques to accurately determine SEI chemistry have also recently been developed, although this is often at the expense of structural information. Fang et al. developed a titration gas chromatography method capable of distinguishing lithium loss due to SEI or dead lithium formation.<sup>10</sup> This was extended by Hobold and Gallant to identify numerous solvent-derived components within the SEI, including lithium alkyl carbonates, organolithium compounds, and Li<sub>2</sub>C<sub>2</sub>. Li<sub>2</sub>C<sub>2</sub> is believed to form through lithium alkyl carbonate reduction, and they found a negative correlation between Li<sub>2</sub>C<sub>2</sub>-content and CE, attributed to its relatively high electronic conductivity.<sup>39</sup> Although it was not identified by the previous two studies,<sup>10,39</sup> other researchers have additionally observed LiH in the SEI.<sup>63,64</sup> LiH can form through solvent decomposition or the reaction of lithium with LiOH, and it can make up a significant proportion of the SEI.<sup>48,65</sup> However, despite these advances in SEI characterization, the majority of the SEI in high CE electrolytes is still unidentified,<sup>39</sup> requiring the further development of techniques capable of quantifying SEI composition with high accuracy.

## Transport

Knowledge of SEI nanostructure alone is currently insufficient to predict cell performance as it is not understood how SEI properties are affected by its structure and composition. The discovery of structure-property relationships would facilitate rational SEI design and guide future electrolyte development and is therefore one of the most pressing avenues for SEI research.

It is important to understand the transport properties of the SEI, as the transport of Li<sup>+</sup> through the SEI determines the rate capability of a cell and controls the morphology of electrodeposited lithium (Figure 3). Maraschky and Akolkar investigated dendrite initiation during lithium electrodeposition and found that dendrites initiate under conditions well below bulk diffusion limitation, with an onset time that decreases with increasing SEI thickness.<sup>23</sup> Analogously to Sand's time,<sup>15</sup> they assumed that a concentration gradient can form within the SEI and that dendrite initiation occurs when the Li<sup>+</sup> concentration at the lithium-SEI interface reaches zero.<sup>23</sup> Dendrites could therefore be prevented by increasing the diffusivity of Li<sup>+</sup>

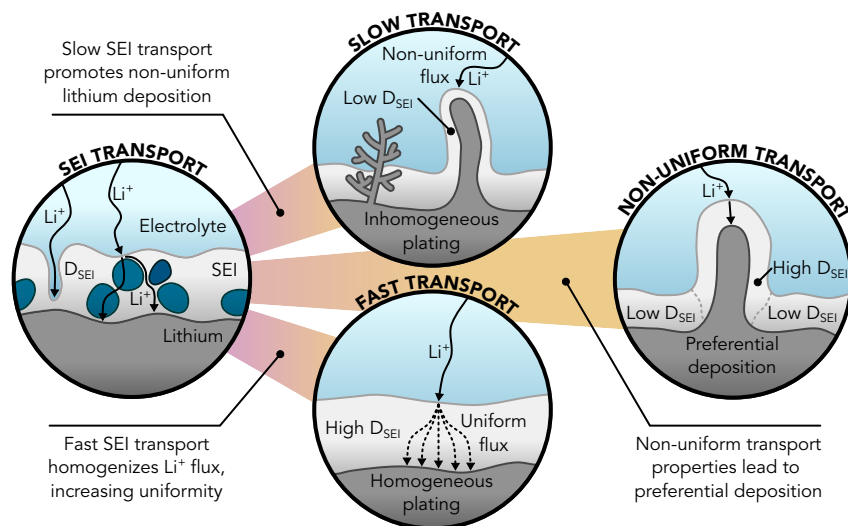


**Figure 3. Solid electrolyte interphase transport**

Schematics of potential solid electrolyte interphase (SEI) transport mechanisms and the influence of SEI transport on lithium deposition morphology. Slow transport can enhance dendrite formation<sup>23</sup> and lead to the formation of mossy lithium.<sup>67</sup> Fast transport enables the homogenization of lithium flux through the SEI, resulting in more uniform deposition.<sup>67</sup> However, preferential lithium deposition will occur below regions with fast transport properties if the SEI is non-uniform, resulting in filamentary deposition.<sup>68</sup>

within the SEI, as demonstrated by an increase in onset time with temperature.<sup>66</sup> However, concentration gradients can only form within the SEI if the cation transference number is below unity; hence, this may only be applicable if the SEI is porous and filled with electrolyte, where both cations and anions are mobile. SEI transport additionally impacts electrodeposition morphology before dendrite initiation. Boyle et al. recently demonstrated that lithium can uniformly plate below the SEI at low current densities ( $\leq 1 \text{ mA cm}^{-2}$ ) and transport through the SEI is the rate-limiting step. However, SEI breakdown can occur at higher current densities, leading to simultaneous lithium plating and SEI formation that results in high-surface-area filamentary deposition, reducing the CE.<sup>67</sup> Improved cycling performance could therefore be achieved by increasing the diffusivity of  $\text{Li}^+$  to enable lithium plating beneath the SEI at higher rates and by designing an SEI with greater resistance to mechanical failure. Furthermore, the diffusivity should not only be high but must be uniform across the SEI to prevent preferentially localized lithium deposition, which can contribute to SEI failure.<sup>68</sup>

There are currently few experimental techniques capable of quantifying transport through the SEI, and it is frequently estimated using electrochemical impedance spectroscopy (EIS). EIS is particularly attractive as it can provide information about the resistance due to charge transfer, the SEI, and diffusion in the electrolyte under real *operando* conditions,<sup>69</sup> although these processes typically overlap, and there is not yet a consensus on how to accurately deconvolve them. Impedance spectra are typically fitted to equivalent circuit models to assign features in the data to physical processes; however, these circuits are not unique.<sup>69</sup> There have therefore been numerous different models proposed to fit impedance data,<sup>40,70–72</sup> many of which only consider the high-frequency data believed to relate to a compact inner SEI layer.<sup>72</sup> It is also often assumed that SEI resistance dominates the impedance; however, Boyle et al. demonstrated that electron charge-transfer resistance can make up as much as 26% of the total interfacial

resistance.<sup>73</sup> Despite the prevalence of EIS in the literature, there has not yet been a comprehensive study to verify the suitability of equivalent circuit models and ensure that apparent physical properties display the expected trends.

The SEI resistance additionally varies with time. Nojabae et al. observed that the interfacial impedance increases with resting time, which they attributed to growth of the SEI by assuming that resistance is directly proportional to SEI thickness.<sup>74</sup> Tracking impedance evolution may therefore give insights into SEI growth kinetics. On the other hand, Lim et al. instead observed that SEI resistance increases during aging as a result of densification, reducing the number of interconnected pores within the SEI that may act as fast-conduction pathways.<sup>41</sup> It is generally believed that the SEI resistance should be minimized, and Hobold et al. recently demonstrated a negative correlation between SEI resistance and CE over a wide range of electrolyte systems.<sup>75</sup> Some of the best-performing electrolytes additionally displayed a significant reduction in impedance during cycling, although it has not yet been established whether this is due to a change in SEI chemistry or an increase in the area of active lithium due to non-uniform deposition. Contrasting results were observed by Boyle et al., who reported no correlation between SEI resistance and CE; however, it should be noted that the EIS and CE measurements were performed under very different SEI formation conditions.<sup>16</sup>

Owing to the difficulty in experimentally measuring the diffusion coefficient of  $\text{Li}^+$  in the SEI, there has been much interest in predictive modeling. Shi et al. combined density functional theory (DFT) with a multiscale diffusion model and developed a “two-layer/two-mechanism” model that considers the transport of  $\text{Li}^+$  through both a porous outer SEI layer and a compact inner layer.<sup>76</sup> They demonstrated that both anions and cations can rapidly move through the porous outer layer, whereas only cations can diffuse through the inner layer, which is the rate-limiting step. Subsequent studies have therefore focused on ion transport through the typical inorganic components of the inner layer ( $\text{Li}_2\text{CO}_3$ ,  $\text{Li}_2\text{O}$ ,  $\text{LiF}$ , and  $\text{LiOH}$ ). Diffusion coefficients have been calculated for transport through bulk phases,<sup>77,78</sup> along grain boundaries and interfaces between components,<sup>79,80</sup> and surface diffusion.<sup>81</sup> However, the predicted diffusion coefficients vary from  $10^{-16}$  to  $10^{-9} \text{ m}^2 \text{ s}^{-1}$  at room temperature, and it is difficult to determine which mechanism is likely to be prevalent without experimental measurements for comparison. Furthermore, real SEIs can differ significantly from simple modeled systems, and SEI components can have very different properties to their bulk counterparts<sup>72</sup>; hence, more accurate characterizations of SEI structure and composition will be required to guide future modeling efforts.

### Mechanical properties

The SEI must be able to resist large volume changes during cycling, and it should be robust enough to support itself without breaking.<sup>82</sup> The SEI also needs to have strong adhesion to both the current collector and lithium metal,<sup>83</sup> with near-perfect wetting required to allow the SEI to be refilled during plating.<sup>49</sup> It is therefore necessary to consider the mechanical properties of the SEI and their influence on cycling performance; although this poses a great experimental challenge.

One popular technique to probe the mechanical properties of the SEI is atomic force microscopy (AFM).<sup>84</sup> It can be used for *in situ* observations of the lithium surface during operation, demonstrating that preferential lithium deposition occurs in regions where the SEI is thinner.<sup>85</sup> A uniform SEI is therefore beneficial to prevent non-uniform filamentary growth, as confirmed by simulations performed by Shen et al.,<sup>86</sup> which also concluded that an SEI elastic modulus above 3 GPa results in optimal



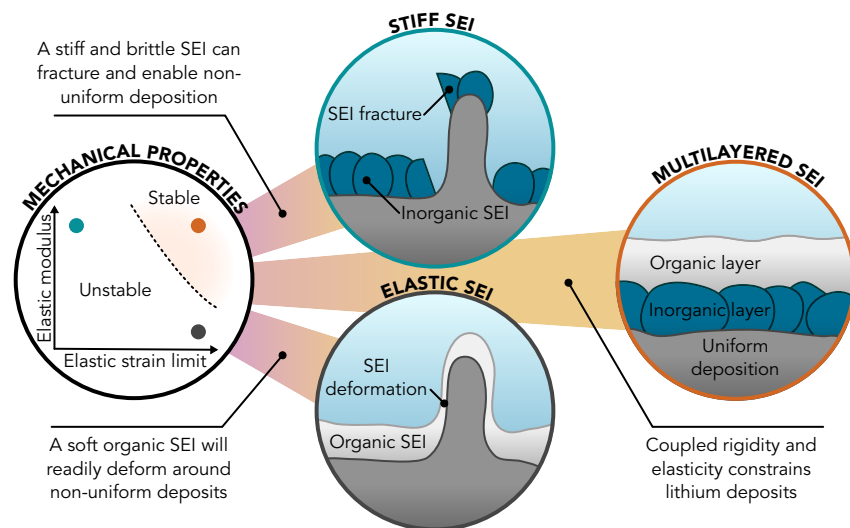


**Figure 4. Solid electrolyte interphase mechanical properties**

Schematic representing the balance of solid electrolyte interphase (SEI) mechanical properties required for stable cycling. A stiff inorganic SEI can be brittle and can fracture at low strain, while a soft organic SEI will readily deform, allowing non-uniform deposition.<sup>92</sup> A combination of inorganic and organic SEI layers affords both rigidity and elasticity, constraining lithium deposits and promoting uniform deposition.<sup>93,95</sup>

stability. Consistent with this, Yuan et al. measured SEI elastic moduli with AFM in a range of electrolytes and observed high CEs when the elastic modulus is above 4 GPa.<sup>87</sup> However, it is challenging to accurately determine the elastic modulus of thin films, and the measured value has been shown to strongly depend on the underlying substrate.<sup>88</sup> To combat this, Yoon et al. prepared model SEI layers on free-standing poly(dimethylsiloxane) (PDMS) substrates. The SEI generated from an ionic liquid electrolyte formed with residual compressive stress, resulting in film buckling with a characteristic wavelength related to the SEI elastic modulus ( $\sim 1$  GPa).<sup>89</sup> In contrast, the SEIs formed in carbonate electrolytes were not under compression, and Yoon et al. used a membrane-bulge configuration to determine the stress-strain behavior, measuring elastic moduli around 200–350 MPa.<sup>90</sup> Reported elastic moduli are therefore prone to uncertainties and can vary by several orders of magnitude. Furthermore, the modulus can change significantly under different sample preparation conditions,<sup>50</sup> requiring the development of techniques capable of accurate mechanical characterization under realistic operating conditions.

The elastic modulus has been the primary focus of many SEI studies, but it is not the only property that impacts cycling performance. Gao et al. used AFM-based nanoindentation to determine the SEI elastic modulus, plus its thickness and elastic strain limit.<sup>91</sup> They observed that CE did not directly correlate with either the elastic modulus or the elastic strain limit, but instead with the maximum elastic deformation energy, which is dependent on both properties. The performance of an SEI therefore not only depends on its rigidity but also on its ability to withstand permanent deformation (Figure 4). Analysis of AFM nanoindentation force curves can also give information about the structure of the SEI, as SEI layers with different properties produce characteristic features.<sup>92</sup> This has been utilized to demonstrate that multilayered SEIs with both organic and inorganic layers result in improved cycling stability,<sup>93,94</sup> likely due to the balance between the rigidity and ductility afforded by the structure.<sup>95</sup> Future work should focus on uncovering the optimal balance of SEI



mechanical properties necessary for stable LMB operation, and how these are related to the nanostructure. This would enable rational SEI design with a consideration of the mechanical and transport properties, providing guidelines for the development of next-generation electrolytes.

## FACTORS AFFECTING THE SEI

### Formation conditions

Determination of accurate SEI nanostructures and properties is further complicated by the fact that the SEI is not uniquely determined by the electrolyte and instead is highly dependent on its formation conditions. Temperature, for example, can have a large impact, and higher temperatures increase the reactivity of lithium metal, generally producing a thicker SEI that degrades cycling performance.<sup>96</sup> However, Wang et al. observed a change in SEI structure at high temperature, forming a  $\text{Li}_2\text{O}$ -rich outer layer that promoted stable cycling.<sup>97</sup> Similarly, a less-resistive SEI can form at low temperatures<sup>98</sup>; hence, LMBs for high- and low-temperature applications could be realized through rational design of electrolyte systems that produce favorable SEIs.

The initial surface of lithium metal is also always covered with a native passivation layer (NPL) composed of  $\text{Li}_2\text{O}$ ,  $\text{Li}_2\text{CO}_3$ , and  $\text{LiOH}$ , although the exact thickness and composition depends on the storage conditions and duration.<sup>99</sup> The NPL influences the resulting SEI that forms on top,<sup>100</sup> making it far more difficult to determine the role of the SEI. To negate the influence of the NPL, Kühn et al. adapted a technique to cut lithium metal electrodes in electrolyte, allowing only SEI to form at the freshly exposed surfaces. The exclusion of the NPL generally reduced impedances and overpotentials, although cycling performance was only improved in one of the systems investigated.<sup>101</sup> Nevertheless, it is important to consider the SEI without the NPL to determine the true impact of electrolyte chemistry on cycling performance and appreciate that the SEI will be highly influenced by any electrode preparation steps prior to cell assembly. Any differences in lithium preparation methods used by different researchers could therefore impact results.

The NPL can also be excluded by electrodeposition of lithium directly onto the current collector<sup>100</sup>; a process that is crucial to the development of zero-excess-lithium cells.<sup>3</sup> However, this introduces additional complexities into SEI analysis, as although lithium metal is able to chemically react with electrolyte species and immediately reduce them, alternative current collectors like copper are unable to reduce the electrolyte in the absence of an applied potential.<sup>102</sup> SEI formation on these higher-electrode-potential substrates instead occurs through electrochemical reduction once the potential of the substrate is reduced below the reduction potential of the electrolyte components.<sup>43,103</sup> As such, SEI nanostructure depends on how the potential is varied during its formation, and it may be very different from that formed on lithium. For example, Wang et al. compared the SEIs formed on copper by linear sweep voltammetry and using a potential step, with a potential step producing a thinner, more inorganic SEI as a result of the lower potential during the entire formation process.<sup>104</sup> Additionally, the SEI that formed on lithium metal was even thinner and more inorganic, and repeated lithium stripping and plating was only observed within SEI shells that formed directly on lithium metal,<sup>104</sup> suggesting that this type of SEI is most beneficial. This is further supported by a recent *in situ* plasmon-enhanced Raman spectroscopy study, which revealed that the initial SEI that forms on copper is restructured after lithium deposition, and performance is enhanced if lithium deposition precedes SEI formation.<sup>105</sup>

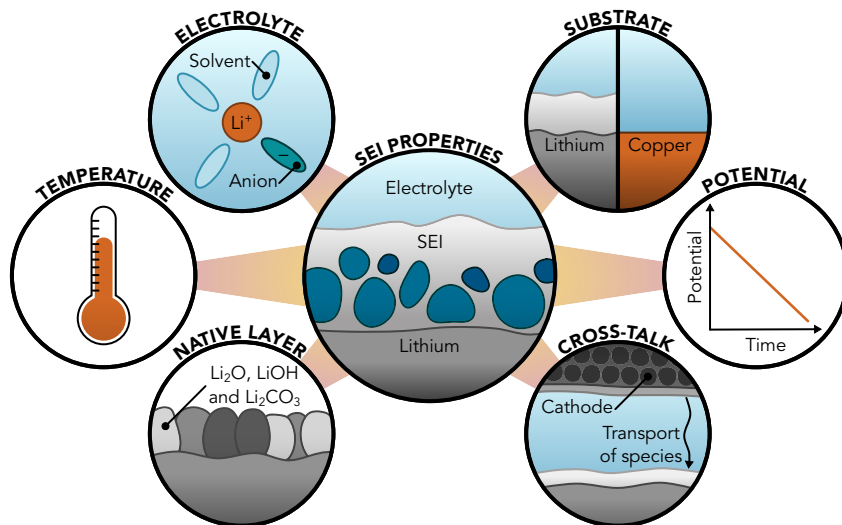


**Figure 5. Factors affecting solid electrolyte interphase nanostructure**

The structure and composition of the solid electrolyte interphase (SEI) is affected by numerous factors, including the electrolyte chemistry and concentration, the temperature during formation, the composition of the native passivation layer on lithium, the choice of substrate material, and the potential of the working electrode during formation. The influence of cross-talk must also be considered when examining full cells.

This electrochemical formation route also offers opportunities to control the structure and chemistry of the SEI, as different electrolyte components undergo reduction at different potentials.<sup>106,107</sup> This could enable the development of formation protocols to produce SEIs with a designed nanostructure by understanding and balancing the thermodynamics and kinetics of the separate reduction reactions.<sup>108</sup> In this way, Gu et al. developed an electrochemical polishing process to control SEI formation while simultaneously generating a near-atomically flat lithium surface,<sup>94</sup> which is beneficial as the SEI is known to mirror the non-uniformities of the underlying substrate,<sup>102,109</sup> producing weak points that can fracture and lead to filament growth.<sup>110</sup> This electrochemical polishing process significantly improved the cycling stability, with a multilayered SEI giving the best performance,<sup>94</sup> possibly due to the formation of a resilient cross-linked organic layer.<sup>111</sup> SEI performance is further influenced by current density during formation and cycling. Oyakhire et al. demonstrated that preforming an SEI with constant current cycling at  $0.5 \text{ mA cm}^{-2}$  (the lowest current density tested) resulted in the highest CE during subsequent cycling.<sup>108</sup> In contrast, Ding et al. reported a reduction in capacity loss due to continuous SEI formation during cycling and an increase in CE when the current density during stripping was increased.<sup>112</sup> The impact of current density on SEI performance therefore requires additional study.

Finally, the SEI can also change dynamically during cycling,<sup>113</sup> with carbonate species observed to form during plating and become partially lost during stripping,<sup>114</sup> likely caused by the non-negligible solubility of most SEI components in typical solvents.<sup>115</sup> Recent evidence further revealed that as much as  $\sim 60\%$  of the mass of the SEI can be lost due to dissolution, and CE was observed to decrease with increasing SEI dissolution.<sup>116</sup> The nanostructure of the SEI is therefore influenced by numerous factors, as summarized in Figure 5, all of which need to be kept as consistent as possible between experiments to ensure that accurate conclusions can be drawn. The implementation of standard SEI formation protocols would also greatly facilitate

the comparison of results obtained by different researchers, accelerating systematic study of the SEI to uncover its role in LMBs.

### Cross-talk

The above discussion applies to the SEI formed in symmetric (Li||Li) or half-cell (Cu||Li) configurations. However, an additional phenomenon must be considered in the case of full cells: cross-talk. Cross-talk describes any process in which (electro)chemical reactions at one electrode produce products that travel to the other electrode and react.<sup>117</sup> One of the more infamous cases of cross-talk occurs when using transition metal oxide cathodes, which suffer from transition metal dissolution. The dissolved metal ions are able to migrate to the anode where they are reduced to form metallic deposits within the SEI, leading to capacity loss.<sup>117,118</sup> The role of dissolved  $\text{Mn}^{2+}$  ions on SEI formation was further investigated by Zhang et al., revealing that the presence of  $\text{Mn}^{2+}$  in the electrolyte alters the electrolyte decomposition reactions and forms a non-uniform manganese-rich SEI, leading to inhomogeneous lithium deposition and significantly reducing the CE.<sup>119</sup> Electrolyte species may also be oxidized at the cathode, generating soluble products that degrade anode performance.<sup>120</sup> On the other hand, cross-talk is not always detrimental.<sup>121</sup> For example,  $\text{CO}_2$  gas generated by electrolyte oxidation at the cathode can be consumed at the anode to form  $\text{Li}_2\text{CO}_3$ , extending cell lifetime.<sup>117</sup> It has also been proposed that high-voltage cathodes can catalyze anion decomposition, forming reactive products that contribute to a favorable SEI on lithium.<sup>65</sup> Understanding the SEI that forms on the anode in full cells therefore requires knowledge of the decomposition reactions occurring at both electrodes, and it presents a significant challenge.

## CRITICAL RESEARCH FRONTS

In this perspective, we have highlighted the importance of the SEI in controlling lithium deposition morphology and cycling stability in LMBs and have discussed the major breakthroughs in understanding the SEI, with a focus on how performance is related to SEI nanostructure, transport, and mechanical properties. However, there still remain unanswered questions that would be instrumental in the rational design of an SEI for safe and stable LMBs. We have therefore identified several critical research fronts (Figure 6) that should be addressed.

### Correlating structure with transport and mechanics

Rational SEI design will first require a determination of the SEI properties needed for stable LMB operation, including  $\text{Li}^+$  diffusivity, elastic modulus, and elastic strain limit. However, methods capable of directly probing  $\text{Li}^+$  transport independently from other processes are currently lacking; hence, their development remains an important challenge. Careful, systematic studies will additionally be necessary to correlate the structure and chemistry of an SEI to its properties, providing guidelines to tailor the performance of an SEI through control of its nanostructure. This would then enable the design of an optimal SEI, further directing the rational development of novel electrolyte formulations and SEI formation protocols capable of achieving this structure, facilitating the commercialization of safe and stable, high-energy-density LMBs.

### Operando characterization techniques

The nanostructure of the SEI can change dynamically during cell operation, and it is strongly influenced by the sample preparation steps used during current post-mortem analysis. This could potentially enable misleading structure-property relationships to direct future research efforts, as may have been the case with the recent interest in a LiF-rich SEI.<sup>57</sup> It is therefore necessary to implement *operando* techniques

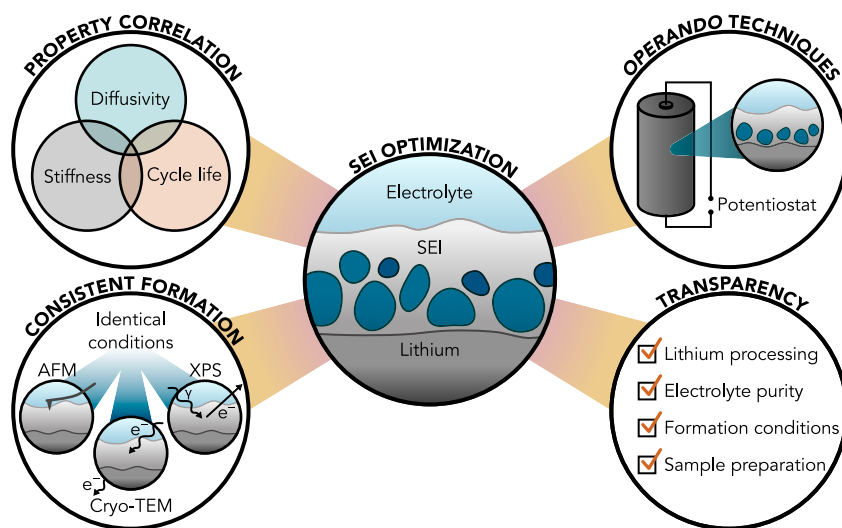


**Figure 6. Critical research fronts for solid electrolyte interphase characterization**

capable of investigating the SEI under realistic operating conditions, allowing its true nanostructure to be determined. To this end, electrochemical techniques, such as EIS, are particularly promising and widely available. Recent developments like dynamic impedance spectroscopy could also offer improved temporal resolution,<sup>122</sup> enabling transient states to be resolved and providing invaluable insights into the mechanisms taking place during SEI formation and cell operation. However, EIS alone cannot give a complete picture of the SEI, requiring the further development of *operando* spectroscopic and tomographic techniques able to probe the SEI with the necessary resolution, such as structured illumination Raman microscopy<sup>123</sup> and ptychographic X-ray laminography.<sup>124</sup>

### Consistent SEI formation

Most current SEI characterization techniques, including cryo-TEM, AFM, and XPS, can only be performed *in situ* or *ex situ*. Although these techniques are unable to probe the SEI during operation, they can still provide useful information about the SEI, particularly when used together, provided the SEI under investigation has been produced consistently. As discussed throughout this perspective, the nanostructure of the SEI is influenced by a wide range of factors, including the lithium surface, temperature, time, potential during formation, and any sample processing steps. All these factors should be kept the same when producing SEI samples for characterization with different techniques to ensure that results from separate experiments can be accurately combined. One potential method of excluding the influence of initial lithium metal topography and surface chemistry is to implement a zero-excess-lithium configuration and form SEI directly on alternative substrates like copper. Although this will be a useful approach for fundamental SEI studies, it is important to note that the SEI formed on copper is likely to differ significantly from that formed on lithium, and as such, they should not be assumed to be equal. Alternatively, the use of different formation protocols on the same electrolyte system could produce several different SEI nanostructures, facilitating the elucidation of the impact of SEI structure on cycling stability without the need to change electrolyte chemistry.

### Transparency in reporting

The wide range of possible SEI formation conditions complicates the comparison of results gathered by different researchers. It is therefore essential that detailed SEI

formation conditions are accurately reported, including any lithium processing, the potential during SEI formation, formation time, and sample preparation steps, as summarized in Figure 5. We further recommend that, where possible, the lithium metal and electrolyte are also characterized. For example, the composition of the NPL on the lithium surface can be examined with XPS, the surface topography can be measured with AFM, and nuclear magnetic resonance (NMR) can be used to verify the purity of electrolyte components. Accurate study of the SEI is a complex problem as all these factors influence its formation and evolution; however, it will be greatly facilitated by thorough reporting that allows all results to be considered in the correct context. We have therefore proposed SEI reporting checklists for both excess-lithium and zero-excess-lithium cells, which are provided in Notes S1 and S2, respectively. Furthermore, the adoption of standard SEI formation protocols would aid the sharing of results between researchers.

## SUPPLEMENTAL INFORMATION

Supplemental information can be found online at <https://doi.org/10.1016/j.joule.2023.08.007>.

## ACKNOWLEDGMENTS

M.P. acknowledges support from the ISCF Faraday Challenge projects SOLBAT (grant number FIRG056) and LiSTAR (grant number FIRG058) as well as the Henry Royce Institute (through UK Engineering and Physical Science Research Council grant EP/R010145/1). B.J. is grateful for the support of the Clarendon Fund Scholarships.

## AUTHOR CONTRIBUTIONS

Conceptualization, B.J. and M.P.; methodology, B.J. and M.P.; investigation, B.J.; writing – original draft, B.J.; writing – review and editing, B.J. and M.P.; visualization, B.J.; funding acquisition, M.P.; supervision, M.P.

## DECLARATION OF INTERESTS

The authors declare no competing interests.

## REFERENCES

- Wang, H., Yu, Z., Kong, X., Kim, S.C., Boyle, D.T., Qin, J., Bao, Z., and Cui, Y. (2022). Liquid electrolyte: the nexus of practical lithium metal batteries. *Joule* 6, 588–616. <https://doi.org/10.1016/j.joule.2021.12.018>.
- Cuberg (2022). Cuberg cell performance validation. <https://www.datocms-assets.com/40252/1659129214-cuberg-cellvalidation-july-2022.pdf>.
- Liu, J., Bao, Z., Cui, Y., Dufek, E.J., Goodenough, J.B., Khalifah, P., Li, Q., Liaw, B.Y., Liu, P., Manthiram, A., et al. (2019). Pathways for practical high-energy long-cycling lithium metal batteries. *Nat. Energy* 4, 180–186. <https://doi.org/10.1038/s41560-019-0338-x>.
- Hobold, G.M., Lopez, J., Guo, R., Minafra, N., Banerjee, A., Meng, Y.S., Shao-Horn, Y., and Gallant, B.M. (2021). Moving beyond 99.9% coulombic efficiency for lithium anodes in liquid electrolytes. *Nat. Energy* 6, 951–960. <https://doi.org/10.1038/s41560-021-00910-w>.
- Xiao, J., Li, Q., Bi, Y., Cai, M., Dunn, B., Glossmann, T., Liu, J., Osaka, T., Sugiura, R., Wu, B., et al. (2020). Understanding and applying coulombic efficiency in lithium metal batteries. *Nat. Energy* 5, 561–568. <https://doi.org/10.1038/s41560-020-0648-z>.
- Albertus, P., Babinec, S., Litzelman, S., and Newman, A. (2018). Status and challenges in enabling the lithium metal electrode for high-energy and low-cost rechargeable batteries. *Nat. Energy* 3, 16–21. <https://doi.org/10.1038/s41560-017-0047-2>.
- Peljo, P., and Girault, H.H. (2018). Electrochemical potential window of battery electrolytes: the HOMO–LUMO misconception. *Energy Environ. Sci.* 11, 2306–2309. <https://doi.org/10.1039/C8EE01286E>.
- Goodenough, J.B., and Kim, Y. (2010). Challenges for rechargeable Li batteries. *Chem. Mater.* 22, 587–603. <https://doi.org/10.1021/cm901452z>.
- Peled, E. (1979). The electrochemical behavior of alkali and alkaline earth metals in nonaqueous battery systems—the solid electrolyte interphase model. *J. Electrochem. Soc.* 126, 2047–2051. <https://doi.org/10.1149/1.2128859>.
- Fang, C., Li, J., Zhang, M., Zhang, Y., Yang, F., Lee, J.Z., Lee, M.-H., Alvarado, J., Schroeder, M.A., Yang, Y., et al. (2019). Quantifying inactive lithium in lithium metal batteries. *Nature* 572, 511–515. <https://doi.org/10.1038/s41586-019-1481-z>.
- Zheng, J., Kim, M.S., Tu, Z., Choudhury, S., Tang, T., and Archer, L.A. (2020). Regulating electrodeposition morphology of lithium: towards commercially relevant secondary Li metal batteries. *Chem. Soc. Rev.* 49, 2701–2750. <https://doi.org/10.1039/c9cs00883g>.
- Fawdon, J., Ihli, J., La Mantia, F., and Pasta, M. (2021). Characterising lithium-ion electrolytes via *operando* Raman microspectroscopy. *Nat. Commun.* 12, 4053. <https://doi.org/10.1038/s41467-021-24297-0>.
- Dhir, S., Jagger, B., Maguire, A., and Pasta, M. (2023). Fundamental investigations on the

- ionic transport and thermodynamic properties of non-aqueous potassium-ion electrolytes. *Nat. Commun.* 14, 3833. <https://doi.org/10.1038/s41467-023-39523-0>.
14. Zhang, X., Wang, A., Liu, X., and Luo, J. (2019). Dendrites in lithium metal anodes: suppression, regulation, and elimination. *Acc. Chem. Res.* 52, 3223–3232. <https://doi.org/10.1021/acs.accounts.9b00437>.
15. Sand, H.J.S. (1899). On the concentration at the electrodes in a solution, with special reference to the liberation of hydrogen by electrolysis of a mixture of copper sulphate and sulphuric acid. *Proc. Phys. Soc. Lond.* 17, 496–534. <https://doi.org/10.1088/1478-7814/17/1/332>.
16. Boyle, D.T., Kim, S.C., Oyakhire, S.T., Vilá, R.A., Huang, Z., Sayavong, P., Qin, J., Bao, Z., and Cui, Y. (2022). Correlating kinetics to cyclability reveals thermodynamic origin of lithium anode morphology in liquid electrolytes. *J. Am. Chem. Soc.* 144, 20717–20725. <https://doi.org/10.1021/jacs.2c08182>.
17. Xu, C., Ahmad, Z., Aryanfar, A., Viswanathan, V., and Greer, J.R. (2017). Enhanced strength and temperature dependence of mechanical properties of Li at small scales and its implications for Li metal anodes. *Proc. Natl. Acad. Sci. USA* 114, 57–61. <https://doi.org/10.1073/pnas.1615733114>.
18. Aspinall, J., Armstrong, D.E.J., and Pasta, M. (2022). EBSD-coupled indentation: nanoscale mechanics of lithium metal. *Mater. Today Energy* 30, 101183. <https://doi.org/10.1016/j.mtener.2022.101183>.
19. Sanchez, A.J., Kazyak, E., Chen, Y., Lasso, J., and Dasgupta, N.P. (2021). Lithium stripping: anisotropic evolution and faceting of pits revealed by *operando* 3-D microscopy. *J. Mater. Chem. A* 9, 21013–21023. <https://doi.org/10.1039/D1TA03333F>.
20. Kasse, R.M., Geise, N.R., Sebt, E., Lim, K., Takacs, C.J., Cao, C., Steinrück, H.-G., and Toney, M.F. (2022). Combined effects of uniform applied pressure and electrolyte additives in lithium-metal batteries. *ACS Appl. Energy Mater.* 5, 8273–8281. <https://doi.org/10.1021/acsaelm.2c00806>.
21. Fang, C., Lu, B., Pawar, G., Zhang, M., Cheng, D., Chen, S., Ceja, M., Doux, J.-M., Musrock, H., Cai, M., et al. (2021). Pressure-tailored lithium deposition and dissolution in lithium metal batteries. *Nat. Energy* 6, 987–994. <https://doi.org/10.1038/s41560-021-00917-3>.
22. Bai, P., Li, J., Brushett, F.R., and Bazant, M.Z. (2016). Transition of lithium growth mechanisms in liquid electrolytes. *Energy Environ. Sci.* 9, 3221–3229. <https://doi.org/10.1039/C6EE01674J>.
23. Maraschky, A., and Akolkar, R. (2018). Mechanism explaining the onset time of dendritic lithium electrodeposition via considerations of the Li<sup>+</sup> transport within the solid electrolyte interphase. *J. Electrochem. Soc.* 165, D696–D703. <https://doi.org/10.1149/2.0601814jes>.
24. Li, Y., Huang, W., Li, Y., Pei, A., Boyle, D.T., and Cui, Y. (2018). Correlating structure and function of battery interphases at atomic resolution using cryoelectron microscopy. *Joule* 2, 2167–2177. <https://doi.org/10.1016/j.joule.2018.08.004>.
25. Cheng, X.-B., Zhang, R., Zhao, C.-Z., and Zhang, Q. (2017). Toward safe lithium metal anode in rechargeable batteries: a review. *Chem. Rev.* 117, 10403–10473. <https://doi.org/10.1021/acs.chemrev.7b00115>.
26. Zhao, Q., Stalin, S., and Archer, L.A. (2021). Stabilizing metal battery anodes through the design of solid electrolyte interphases. *Joule* 5, 1119–1142. <https://doi.org/10.1016/j.joule.2021.03.024>.
27. Gong, C., Pu, S.D., Gao, X., Yang, S., Liu, J., Ning, Z., Rees, G.J., Capone, I., Pi, L., Liu, B., et al. (2021). Revealing the role of fluoride-rich battery electrode interphases by *operando* transmission electron microscopy. *Adv. Energy Mater.* 11, 2003118. <https://doi.org/10.1002/aenm.202003118>.
28. Alvarado, J., Schroeder, M.A., Pollard, T.P., Wang, X., Lee, J.Z., Zhang, M., Wynn, T., Ding, M., Borodin, O., Meng, Y.S., et al. (2019). Bisalt ether electrolytes: A pathway towards lithium metal batteries with Ni-Rich cathodes. *Energy Environ. Sci.* 12, 780–794. <https://doi.org/10.1039/C8EE02601G>.
29. Yu, Z., Balsara, N.P., Borodin, O., Gewirth, A.A., Hahn, N.T., Maginn, E.J., Persson, K.A., Srinivasan, V., Toney, M.F., Xu, K., et al. (2022). Beyond local solvation structure: nanometric aggregates in battery electrolytes and their effect on electrolyte properties. *ACS Energy Lett.* 7, 461–470. <https://doi.org/10.1021/acsenenergylett.1c02391>.
30. Cao, X., Jia, H., Xu, W., and Zhang, J.-G. (2021). Review—localized high-concentration electrolytes for lithium batteries. *J. Electrochem. Soc.* 168, 010522. <https://doi.org/10.1149/1945-7111/abd60e>.
31. Jang, J., Sugimoto, T., Mizumo, T., Lee, J.-M., Chang, W.-S., and Mun, J. (2021). High-voltage-compatible dual-ether electrolyte for lithium metal batteries. *ACS Appl. Energy Mater.* 4, 9032–9037. <https://doi.org/10.1021/acsaelm.1c01322>.
32. Feng, X., Zhang, Z., Li, R., Xiong, W., Yu, B., Wang, M., Chen, J., Ma, Z., Guo, B., Huang, Y., et al. (2022). New nonflammable tributyl phosphate based localized high concentration electrolytes for lithium metal batteries. *Sustain. Energy Fuels* 6, 2198–2206. <https://doi.org/10.1039/D2SE00231K>.
33. Zheng, X., Huang, L., Luo, W., Wang, H., Dai, Y., Liu, X., Wang, Z., Zheng, H., and Huang, Y. (2021). Tailoring electrolyte solvation chemistry toward an inorganic-rich solid-electrolyte interphase at a Li metal anode. *ACS Energy Lett.* 6, 2054–2063. <https://doi.org/10.1021/acsenenergylett.1c00647>.
34. Zhang, X.-Q., Cheng, X.-B., Chen, X., Yan, C., and Zhang, Q. (2017). Fluoroethylene carbonate additives to render uniform Li deposits in lithium metal batteries. *Adv. Funct. Mater.* 27, 1605989. <https://doi.org/10.1002/adfm.201605989>.
35. Olana, B.N., Lin, S.D., and Hwang, B.-J. (2022). *In situ* diffuse reflectance infrared Fourier-transformed spectroscopy study of solid electrolyte interphase formation from lithium bis(trifluoromethanesulfonyl)imide in 1,2-dimethoxyethane and 1,3-dioxolane with and without lithium nitrate additive over lithium and copper metal anodes. *Electrochim. Acta* 416, 140266. <https://doi.org/10.1016/j.electacta.2022.140266>.
36. Yoshii, K., Kiuchi, H., Taguchi, N., Shikano, M., Matsubara, E., and Sakaebe, H. (2020). Effects of film formation on the electrodeposition of lithium. *ChemElectroChem* 7, 4336–4342. <https://doi.org/10.1002/celec.202001037>.
37. Xu, R., Cheng, X.-B., Yan, C., Zhang, X.-Q., Xiao, Y., Zhao, C.-Z., Huang, J.-Q., and Zhang, Q. (2019). Artificial interphases for highly stable lithium metal anode. *Matter* 1, 317–344. <https://doi.org/10.1016/j.matt.2019.05.016>.
38. Zhang, W., Zhang, S., Fan, L., Gao, L., Kong, X., Li, S., Li, J., Hong, X., and Lu, Y. (2019). Tuning the LUMO energy of an organic interphase to stabilize lithium metal batteries. *ACS Energy Lett.* 4, 644–650. <https://doi.org/10.1021/acsenenergylett.8b02483>.
39. Hobold, G.M., and Gallant, B.M. (2022). Quantifying capacity loss mechanisms of Li metal anodes beyond inactive Li<sup>0</sup>. *ACS Energy Lett.* 7, 3458–3466. <https://doi.org/10.1021/acsenenergylett.2c01845>.
40. Peled, E., Golodnitsky, D., and Ardel, G. (1997). Advanced model for solid electrolyte interphase electrodes in liquid and polymer electrolytes. *J. Electrochem. Soc.* 144, L208–L210. <https://doi.org/10.1149/1.1837858>.
41. Lim, K., Fenk, B., Popovic, J., and Maier, J. (2021). Porosity of solid electrolyte interphases on alkali metal electrodes with liquid electrolytes. *ACS Appl. Mater. Interfaces* 13, 51767–51774. <https://doi.org/10.1021/acsami.1c15607>.
42. Ma, C., Xu, F., and Song, T. (2022). Dual-layered interfacial evolution of lithium metal anode: SEI analysis via TOF-SIMS technology. *ACS Appl. Mater. Interfaces* 14, 20197–20207. <https://doi.org/10.1021/acsami.2c00842>.
43. Zhou, Y., Su, M., Yu, X., Zhang, Y., Wang, J.G., Ren, X., Cao, R., Xu, W., Baer, D.R., Du, Y., et al. (2020). Real-time mass spectrometric characterization of the solid-electrolyte interphase of a lithium-ion battery. *Nat. Nanotechnol.* 15, 224–230. <https://doi.org/10.1038/s41565-019-0618-4>.
44. Li, Y., Li, Y., Pei, A., Yan, K., Sun, Y., Wu, C.-L., Joubert, L.-M., Chin, R., Koh, A.L., Yu, Y., et al. (2017). Atomic structure of sensitive battery materials and interfaces revealed by cryo-electron microscopy. *Science* 358, 506–510. <https://doi.org/10.1126/science.aam6014>.
45. Cao, X., Ren, X., Zou, L., Engelhard, M.H., Huang, W., Wang, H., Matthews, B.E., Lee, H., Niu, C., Arey, B.W., et al. (2019). Monolithic solid-electrolyte interphases formed in fluorinated orthoformate-based electrolytes minimize Li depletion and pulverization. *Nat. Energy* 4, 796–805. <https://doi.org/10.1038/s41560-019-0464-5>.
46. Yu, Z., Wang, H., Kong, X., Huang, W., Tsao, Y., Mackanic, D.G., Wang, K., Wang, X., Huang, W., Choudhury, S., et al. (2020). Molecular design for electrolyte solvents enabling energy-dense and long-cycling lithium metal batteries. *Nat. Energy* 5,



- 526–533. <https://doi.org/10.1038/s41560-020-0634-5>.
47. Han, B., Zhang, Z., Zou, Y., Xu, K., Xu, G., Wang, H., Meng, H., Deng, Y., Li, J., and Gu, M. (2021). Poor stability of  $\text{Li}_2\text{CO}_3$  in the solid electrolyte interphase of a lithium-metal anode revealed by cryo-electron microscopy. *Adv. Mater.* 33, e2100404. <https://doi.org/10.1002/adma.202100404>.
48. Zachman, M.J., Tu, Z., Choudhury, S., Archer, L.A., and Kourkoutis, L.F. (2018). Cryo-STEM mapping of solid-liquid interfaces and dendrites in lithium-metal batteries. *Nature* 560, 345–349. <https://doi.org/10.1038/s41586-018-0397-3>.
49. Han, B., Li, X., Wang, Q., Zou, Y., Xu, G., Cheng, Y., Zhang, Z., Zhao, Y., Deng, Y., Li, J., et al. (2022). Cryo-electron tomography of highly deformable and adherent solid-electrolyte interphase exoskeleton in Li-metal batteries with ether-based electrolyte. *Adv. Mater.* 34, e2108252. <https://doi.org/10.1002/adma.202108252>.
50. Zhang, Z., Li, Y., Xu, R., Zhou, W., Li, Y., Oyakhire, S.T., Wu, Y., Xu, J., Wang, H., Yu, Z., et al. (2022). Capturing the swelling of solid-electrolyte interphase in lithium metal batteries. *Science* 375, 66–70. <https://doi.org/10.1126/science.abi8703>.
51. Oyakhire, S.T., Gong, H., Cui, Y., Bao, Z., and Bent, S.F. (2022). An X-ray photoelectron spectroscopy primer for solid electrolyte interphase characterization in lithium metal anodes. *ACS Energy Lett.* 7, 2540–2546. <https://doi.org/10.1021/acsenergylett.2c01227>.
52. Tan, J., Matz, J., Dong, P., Shen, J., and Ye, M. (2021). A growing appreciation for the role of LiF in the solid electrolyte interphase. *Adv. Energy Mater.* 11, 2100046. <https://doi.org/10.1002/aenm.202100046>.
53. Yu, W., Yu, Z., Cui, Y., and Bao, Z. (2022). Degradation and speciation of Li salts during XPS analysis for battery research. *ACS Energy Lett.* 7, 3270–3275. <https://doi.org/10.1021/acsenergylett.2c01587>.
54. Brundle, C.R., Crist, B.V., and Bagus, P.S. (2021). Accuracy limitations for composition analysis by XPS using relative peak intensities: LiF as an example. *J. Vac. Sci. Technol. A* 39, 013202. <https://doi.org/10.1116/6.0000674>.
55. Wi, S., Shutthanandan, V., Sivakumar, B.M., Thevuthasan, S., Prabhakaran, V., Roy, S., Karakoti, A., and Murugesan, V. (2022). *In situ* X-ray photoelectron spectroscopy analysis of electrochemical interfaces in battery: recent advances and remaining challenges. *J. Vac. Sci. Technol. A* 40, 010808. <https://doi.org/10.1116/6.0001460>.
56. Narayanan, S., Gibson, J.S., Aspinall, J., Weatherup, R.S., and Pasta, M. (2022). *In situ* and *operando* characterisation of Li metal – solid electrolyte interfaces. *Curr. Opin. Solid State Mater. Sci.* 26, 100978. <https://doi.org/10.1016/j.cossms.2021.100978>.
57. Huang, W., Wang, H., Boyle, D.T., Li, Y., and Cui, Y. (2020). Resolving nanoscopic and mesoscopic heterogeneity of fluorinated species in battery solid-electrolyte interphases by cryogenic electron microscopy. *ACS Energy Lett.* 5, 1128–1135. <https://doi.org/10.1021/acsenergylett.0c00194>.
58. Brown, Z.L., Jurng, S., Nguyen, C.C., and Lucht, B.L. (2018). Effect of fluoroethylene carbonate electrolytes on the nanostructure of the solid electrolyte interphase and performance of lithium metal anodes. *ACS Appl. Energy Mater.* 1, 3057–3062. <https://doi.org/10.1021/acsaem.8b00705>.
59. Jurng, S., Brown, Z.L., Kim, J., and Lucht, B.L. (2018). Effect of electrolyte on the nanostructure of the solid electrolyte interphase (SEI) and performance of lithium metal anodes. *Energy Environ. Sci.* 11, 2600–2608. <https://doi.org/10.1039/C8EE00364E>.
60. He, M., Guo, R., Hobold, G.M., Gao, H., and Gallant, B.M. (2020). The intrinsic behavior of lithium fluoride in solid electrolyte interphases on lithium. *Proc. Natl. Acad. Sci. USA* 117, 73–79. <https://doi.org/10.1073/pnas.1911017116>.
61. Kim, S.C., Kong, X., Vilá, R.A., Huang, W., Chen, Y., Boyle, D.T., Yu, Z., Wang, H., Bao, Z., Qin, J., et al. (2021). Potentiometric measurement to probe solvation energy and its correlation to lithium battery cyclability. *J. Am. Chem. Soc.* 143, 10301–10308. <https://doi.org/10.1021/jacs.1c03868>.
62. Ko, S., Obukata, T., Shimada, T., Takenaka, N., Nakayama, M., Yamada, A., and Yamada, Y. (2022). Electrode potential influences the reversibility of lithium-metal anodes. *Nat. Energy* 7, 1217–1224. <https://doi.org/10.1038/s41560-022-01144-0>.
63. Shadike, Z., Lee, H., Borodin, O., Cao, X., Fan, X., Wang, X., Lin, R., Bak, S.M., Ghose, S., Xu, K., et al. (2021). Identification of LiH and nanocrystalline LiF in the solid-electrolyte interphase of lithium metal anodes. *Nat. Nanotechnol.* 16, 549–554. <https://doi.org/10.1038/s41565-020-00845-5>.
64. Tao, M., Xiang, Y., Zhao, D., Shan, P., Sun, Y., and Yang, Y. (2022). Quantifying the evolution of inactive Li/lithium hydride and their correlations in rechargeable anode-free Li batteries. *Nano Lett.* 22, 6775–6781. <https://doi.org/10.1021/acs.nanolett.2c02484>.
65. Tan, S., Kim, J.M., Corrao, A., Ghose, S., Zhong, H., Rui, N., Wang, X., Senanayake, S., Polzin, B.J., Khalifah, P., et al. (2023). Unravelling the convoluted and dynamic interphasial mechanisms on Li metal anodes. *Nat. Nanotechnol.* 18, 243–249. <https://doi.org/10.1038/s41565-022-01273-3>.
66. Maraschky, A., and Akolkar, R. (2020). Temperature dependence of dendritic lithium electrodeposition: A mechanistic study of the role of transport limitations within the SEI. *J. Electrochem. Soc.* 167, 062503. <https://doi.org/10.1149/1945-7111/ab7ce2>.
67. Boyle, D.T., Li, Y., Pei, A., Vilá, R.A., Zhang, Z., Sayavong, P., Kim, M.S., Huang, W., Wang, H., Liu, Y., et al. (2022). Resolving current-dependent regimes of electroplating mechanisms for fast charging lithium metal anodes. *Nano Lett.* 22, 8224–8232. <https://doi.org/10.1021/acs.nanolett.2c02792>.
68. Zhang, S., Li, R., Hu, N., Deng, T., Weng, S., Wu, Z., Lu, D., Zhang, H., Zhang, J., Wang, X., et al. (2022). Tackling realistic  $\text{Li}^+$  flux for high-energy lithium metal batteries. *Nat. Commun.* 13, 5431. <https://doi.org/10.1038/s41467-022-33151-w>.
69. Vivier, V., and Orazem, M.E. (2022). Impedance analysis of electrochemical systems. *Chem. Rev.* 122, 11131–11168. <https://doi.org/10.1021/acs.chemrev.1c00876>.
70. Zaban, A., Zinigrad, E., and Aurbach, D. (1996). Impedance spectroscopy of Li electrodes. 4. A General Simple Model of the Li-solution interphase in polar aprotic systems. *J. Phys. Chem.* 100, 3089–3101. <https://doi.org/10.1021/jp9514279>.
71. Single, F., Horstmann, B., and Latz, A. (2019). Theory of impedance spectroscopy for lithium batteries. *J. Phys. Chem. C* 123, 27327–27343. <https://doi.org/10.1021/acs.jpcc.9b07389>.
72. Guo, R., and Gallant, B.M. (2020).  $\text{Li}_2\text{O}$  solid electrolyte interphase: probing transport properties at the chemical potential of lithium. *Chem. Mater.* 32, 5525–5533. <https://doi.org/10.1021/acs.chemmater.0c00333>.
73. Boyle, D.T., Kong, X., Pei, A., Rudnicki, P.E., Shi, F., Huang, W., Bao, Z., Qin, J., and Cui, Y. (2020). Transient voltammetry with ultramicroelectrodes reveals the electron transfer kinetics of lithium metal anodes. *ACS Energy Lett.* 5, 701–709. <https://doi.org/10.1021/acsenergylett.0c00031>.
74. Nojabaei, M., Küster, K., Starke, U., Popovic, J., and Maier, J. (2020). Solid electrolyte interphase evolution on lithium metal in contact with glyme-based electrolytes. *Small* 16, e2000756. <https://doi.org/10.1002/sml.202000756>.
75. Hobold, G.M., Kim, K.-H., and Gallant, B.M. (2023). Beneficial vs. inhibiting Passivation by the Native lithium Solid Electrolyte Interphase Revealed by Electrochemical  $\text{Li}^+$  Exchange. *Energy Environ. Sci.* 16, 2247–2261. <https://doi.org/10.1039/D2EE04203G>.
76. Shi, S., Lu, P., Liu, Z., Qi, Y., Hector, L.G., Li, H., and Harris, S.J. (2012). Direct calculation of Li-ion transport in the solid electrolyte interphase. *J. Am. Chem. Soc.* 134, 15476–15487. <https://doi.org/10.1021/ja305366r>.
77. Benitez, L., and Seminario, J.M. (2017). Ion diffusivity through the solid electrolyte interphase in lithium-ion batteries. *J. Electrochem. Soc.* 164, E3159–E3170. <https://doi.org/10.1149/2.0181711jes>.
78. Lanjan, A., Moradi, Z., and Srinivasan, S. (2021). Multiscale investigation of the diffusion mechanism within the solid-electrolyte interface layer: coupling quantum mechanics, molecular dynamics, and macroscale mathematical modeling. *ACS Appl. Mater. Interfaces* 13, 42220–42229. <https://doi.org/10.1021/acsami.1c12322>.
79. Ramasubramanian, A., Yurkiv, V., Foroozan, T., Ragone, M., Shahbazian-Yassar, R., and Mashayek, F. (2019). Lithium diffusion mechanism through solid–electrolyte interphase in rechargeable lithium batteries. *J. Phys. Chem. C* 123, 10237–10245. <https://doi.org/10.1021/acs.jpcc.9b00436>.



80. Ahmad, Z., Venturi, V., Hafiz, H., and Viswanathan, V. (2021). Interfaces in solid electrolyte interphase: implications for lithium-ion batteries. *J. Phys. Chem. C* 125, 11301–11309. <https://doi.org/10.1021/acs.jpcc.1c00867>.
81. Zheng, J., Ju, Z., Zhang, B., Nai, J., Liu, T., Liu, Y., Xie, Q., Zhang, W., Wang, Y., and Tao, X. (2021). Lithium ion diffusion mechanism on the inorganic components of the solid-electrolyte interphase. *J. Mater. Chem. A* 9, 10251–10259. <https://doi.org/10.1039/D0TA11444H>.
82. McBrayer, J.D., Apblett, C.A., Harrison, K.L., Fenton, K.R., and Minter, S.D. (2021). Mechanical studies of the solid electrolyte interphase on anodes in lithium and lithium ion batteries. *Nanotechnology* 32, 502005. <https://doi.org/10.1088/1361-6528/ac17fe>.
83. Lee, S.-Y., Shangguan, J., Betzler, S., Harris, S.J., Doeff, M.M., and Zheng, H. (2022). Lithium metal stripping mechanisms revealed through electrochemical liquid cell electron microscopy. *Nano Energy* 102, 107641. <https://doi.org/10.1016/j.nanoen.2022.107641>.
84. Wang, W.-W., Gu, Y., Wang, J.-H., Chen, Z.-B., Yin, X.-T., Wu, Q.-H., Yan, J.-W., and Mao, B.-W. (2022). Probing mechanical properties of solid-electrolyte interphases on Li nuclei by *in situ* AFM. *J. Electrochem. Soc.* 169, 020563. <https://doi.org/10.1149/1945-7111/ac53d0>.
85. Kitta, M., and Sano, H. (2017). Real-time observation of Li deposition on a Li electrode with *operando* atomic force microscopy and surface mechanical imaging. *Langmuir* 33, 1861–1866. <https://doi.org/10.1021/acs.langmuir.6b04651>.
86. Shen, X., Zhang, R., Chen, X., Cheng, X.-B., Li, X., and Zhang, Q. (2020). The failure of solid electrolyte interphase on Li metal anode: structural uniformity or mechanical strength? *Adv. Energy Mater.* 10, 1903645. <https://doi.org/10.1002/aenm.201903645>.
87. Yuan, S., Weng, S., Wang, F., Dong, X., Wang, Y., Wang, Z., Shen, C., Bao, J.L., Wang, X., and Xia, Y. (2021). Revisiting the designing criteria of advanced solid electrolyte interphase on lithium metal anode under practical condition. *Nano Energy* 83, 105847. <https://doi.org/10.1016/j.nanoen.2021.105847>.
88. Saha, R., and Nix, W.D. (2002). Effects of the substrate on the determination of thin film mechanical properties by nanoindentation. *Acta Mater.* 50, 23–38. [https://doi.org/10.1016/S1359-6454\(01\)00328-7](https://doi.org/10.1016/S1359-6454(01)00328-7).
89. Yoon, I., Jurng, S., Abraham, D.P., Lucht, B.L., and Guduru, P.R. (2018). *In situ* measurement of the plane-strain modulus of the solid electrolyte interphase on lithium-metal anodes in ionic liquid electrolytes. *Nano Lett.* 18, 5752–5759. <https://doi.org/10.1021/acs.nanolett.8b02363>.
90. Yoon, I., Jurng, S., Abraham, D.P., Lucht, B.L., and Guduru, P.R. (2020). Measurement of mechanical and fracture properties of solid electrolyte interphase on lithium metal anodes in lithium ion batteries. *Energy Storage Mater.* 25, 296–304. <https://doi.org/10.1016/j.ensm.2019.10.009>.
91. Gao, Y., Du, X., Hou, Z., Shen, X., Mai, Y.-W., Tarascon, J.-M., and Zhang, B. (2021). Unraveling the mechanical origin of stable solid electrolyte interphase. *Joule* 5, 1860–1872. <https://doi.org/10.1016/j.joule.2021.05.015>.
92. Wang, W.-W., Gu, Y., Yan, H., Li, S., He, J.-W., Xu, H.-Y., Wu, Q.-H., Yan, J.-W., and Mao, B.-W. (2020). Evaluating solid-electrolyte interphases for lithium and lithium-free anodes from nanoindentation features. *Chem* 6, 2728–2745. <https://doi.org/10.1016/j.chempr.2020.07.014>.
93. Wang, J., Yang, J., Xiao, Q., Zhang, J., Li, T., Jia, L., Wang, Z., Cheng, S., Li, L., Liu, M., et al. (2021). *In situ* self-assembly of ordered organic/inorganic dual-layered interphase for achieving long-life dendrite-free Li metal anodes in LiFSI-based electrolyte. *Adv. Funct. Mater.* 31, 2007434. <https://doi.org/10.1002/adfm.202007434>.
94. Gu, Y., Wang, W.-W., Li, Y.-J., Wu, Q.-H., Tang, S., Yan, J.-W., Zheng, M.-S., Wu, D.-Y., Fan, C.-H., Hu, W.-Q., et al. (2018). Designable ultra-smooth ultra-thin solid-electrolyte interphases of three alkali metal anodes. *Nat. Commun.* 9, 1339. <https://doi.org/10.1038/s41467-018-03466-8>.
95. Zhang, Q.-K., Zhang, X.-Q., Wan, J., Yao, N., Song, T.-L., Xie, J., Hou, L.-P., Zhou, M.-Y., Chen, X., Li, B.-Q., et al. (2023). Homogeneous and mechanically stable solid-electrolyte interphase enabled by trioxane-modulated electrolytes for lithium metal batteries. *Nat. Energy* 8, 725–735. <https://doi.org/10.1038/s41560-023-01275-y>.
96. Boroujeni, S.M., Fill, A., Ridder, A., and Birke, K.P. (2021). Influence of temperature and electrolyte composition on the performance of lithium metal anodes. *Batteries* 7, 67. <https://doi.org/10.3390/batteries7040067>.
97. Wang, J., Huang, W., Pei, A., Li, Y., Shi, F., Yu, X., and Cui, Y. (2019). Improving cyclability of Li metal batteries at elevated temperatures and its origin revealed by cryo-electron microscopy. *Nat. Energy* 4, 664–670. <https://doi.org/10.1038/s41560-019-0413-3>.
98. Thenuwara, A.C., Shetty, P.P., and McDowell, M.T. (2019). Distinct nanoscale interphases and morphology of lithium metal electrodes operating at low temperatures. *Nano Lett.* 19, 8664–8672. <https://doi.org/10.1021/acs.nanolett.9b03330>.
99. Otto, S.K., Moryson, Y., Krauskopf, T., Peppeler, K., Sann, J., Janek, J., and Henss, A. (2021). In-depth characterization of lithium-metal surfaces with XPS and ToF-SIMS: toward better understanding of the passivation layer. *Chem. Mater.* 33, 859–867. <https://doi.org/10.1021/acs.chemmater.0c03518>.
100. Haas, R., and Janek, J. (2022). The influence of oxygen dissolved in the liquid electrolyte on lithium metal anodes. *J. Electrochem. Soc.* 169, 110527. <https://doi.org/10.1149/1945-7111/ac9d6b>.
101. Kühn, S.P., Pfeiffer, F., Bela, M., Rodehorst, U., Weintz, D., Stan, M., Baghernejad, M., Winter, M., and Cekic-Laskovic, I. (2022). Back to the basics: advanced understanding of the as-defined solid electrolyte interphase on lithium metal electrodes. *J. Power Sources* 549, 232118. <https://doi.org/10.1016/j.jpowsour.2022.232118>.
102. Xu, Y., Wu, H., Jia, H., Engelhard, M.H., Zhang, J.-G., Xu, W., and Wang, C. (2020). Sweeping potential regulated structural and chemical evolution of solid-electrolyte interphase on Cu and Li as revealed by cryo-TEM. *Nano Energy* 76, 105040. <https://doi.org/10.1016/j.nanoen.2020.105040>.
103. Liu, J., Pei, N., Hua, H., Deng, Y., Ma, H., Zhang, P., and Zhao, J. (2022). From mosaic-type to heterojunction-type SEI films on the Li anode: decoupling chemical and electrochemical degradation of the electrolyte. *ACS Sustainable Chem. Eng.* 10, 9232–9241. <https://doi.org/10.1021/acscuschemeng.2c02668>.
104. Wang, W.-W., Gu, Y., Yan, H., Li, K.-X., Chen, Z.-B., Wu, Q.-H., Kranz, C., Yan, J.-W., and Mao, B.-W. (2022). Formation sequence of solid electrolyte interphases and impacts on lithium deposition and dissolution on copper: an *in situ* atomic force microscopic study. *Faraday Discuss.* 233, 190–205. <https://doi.org/10.1039/d1fd00043h>.
105. Gu, Y., You, E.-M., Lin, J.-D., Wang, J.-H., Luo, S.-H., Zhou, R.-Y., Zhang, C.-J., Yao, J.-L., Li, H.-Y., Li, G., et al. (2023). Resolving nanostructure and chemistry of solid-electrolyte interphase on lithium anodes by depth-sensitive plasmon-enhanced Raman spectroscopy. *Nat. Commun.* 14, 3536. <https://doi.org/10.1038/s41467-023-39192-z>.
106. Cao, C., Pollard, T.P., Borodin, O., Mars, J.E., Tsao, Y., Lukatskaya, M.R., Kasse, R.M., Schroeder, M.A., Xu, K., Toney, M.F., et al. (2021). Toward unraveling the origin of lithium fluoride in the solid electrolyte interphase. *Chem. Mater.* 33, 7315–7336. <https://doi.org/10.1021/acs.chemmater.1c01744>.
107. Shin, W., and Manthiram, A. (2022). A facile potential hold method for fostering an inorganic solid-electrolyte interphase for anode-free lithium-metal batteries. *Angew. Chem. Int. Ed. Engl.* 61, e202115909. <https://doi.org/10.1002/anie.202115909>.
108. Oyakhire, S.T., Zhang, W., Yu, Z., Holmes, S.E., Sayavong, P., Kim, S.C., Boyle, D.T., Kim, M.S., Zhang, Z., Cui, Y., et al. (2023). Correlating the formation protocols of solid electrolyte interphases with practical performance metrics in lithium metal batteries. *ACS Energy Lett.* 8, 869–877. <https://doi.org/10.1021/acsenergylett.2c02137>.
109. Shi, F., Pei, A., Boyle, D.T., Xie, J., Yu, X., Zhang, X., and Cui, Y. (2018). Lithium metal stripping beneath the solid electrolyte interphase. *Proc. Natl. Acad. Sci. USA* 115, 8529–8534. <https://doi.org/10.1073/pnas.1806878115>.
110. Aurbach, D., Zinigrad, E., Cohen, Y., and Teller, H. (2002). A short review of failure mechanisms of lithium metal and lithiated graphite anodes in liquid electrolyte solutions. *Solid State Ion.* 148, 405–416. [https://doi.org/10.1016/S0167-2738\(02\)00080-2](https://doi.org/10.1016/S0167-2738(02)00080-2).
111. Gu, Y., Wang, W.-W., He, J.-W., Tang, S., Xu, H.-Y., Yan, J.-W., Wu, Q.-H., Lian, X.-B., Zheng, M.-S., Dong, Q.-F., et al. (2019).

- Electrochemical polishing of lithium metal surface for highly demanding solid-electrolyte interphase. *ChemElectroChem* 6, 181–188. <https://doi.org/10.1002/celec.201800907>.
112. Ding, J.-F., Xu, R., Xiao, Y., Zhang, S., Song, T.-L., Yan, C., and Huang, J.-Q. (2023). Dynamic galvanic corrosion of working lithium metal anode under practical conditions. *Adv. Energy Mater.* 13, 2204305. <https://doi.org/10.1002/aenm.202204305>.
  113. Guo, R., Wang, D., Zuin, L., and Gallant, B.M. (2021). Reactivity and evolution of ionic phases in the lithium solid–electrolyte interphase. *ACS Energy Lett.* 6, 877–885. <https://doi.org/10.1021/acseenergylett.1c00117>.
  114. Zhuo, Z., Lu, P., Delacourt, C., Qiao, R., Xu, K., Pan, F., Harris, S.J., and Yang, W. (2018). Breathing and oscillating growth of solid-electrolyte-interphase upon electrochemical cycling. *Chem. Commun.* 54, 814–817. <https://doi.org/10.1039/c7cc07082a>.
  115. Tasaki, K., Goldberg, A., Lian, J.-J., Walker, M., Timmons, A., and Harris, S.J. (2009). Solubility of lithium salts formed on the lithium-ion battery negative electrode surface in organic solvents. *J. Electrochem. Soc.* 156, A1019. <https://doi.org/10.1149/1.3239850>.
  116. Sayavong, P., Zhang, W., Oyakhire, S.T., Boyle, D.T., Chen, Y., Kim, S.C., Vilá, R.A., Holmes, S.E., Kim, M.S., Bent, S.F., et al. (2023). Dissolution of the solid electrolyte interphase and its effects on lithium metal anode cyclability. *J. Am. Chem. Soc.* 145, 12342–12350. <https://doi.org/10.1021/jacs.3c03195>.
  117. Harris, O.C., Lee, S.E., Lees, C., and Tang, M. (2020). Review: mechanisms and consequences of chemical cross-talk in advanced Li-ion batteries. *J. Phys. Energy* 2, 032002. <https://doi.org/10.1088/2515-7655/ab8b68>.
  118. Betz, J., Brinkmann, J.-P., Nölle, R., Lürenbaum, C., Kolek, M., Stan, M.C., Winter, M., and Placke, T. (2019). Cross talk between transition metal cathode and Li metal anode: unraveling its influence on the deposition/dissolution behavior and morphology of lithium. *Adv. Energy Mater.* 9, 1900574. <https://doi.org/10.1002/aenm.201900574>.
  119. Zhang, X.-Q., Wang, X.-M., Li, B.-Q., Shi, P., Huang, J.-Q., Chen, A., and Zhang, Q. (2020). Crosstalk shielding of transition metal ions for long cycling lithium–metal batteries. *J. Mater. Chem. A* 8, 4283–4289. <https://doi.org/10.1039/C9TA12269A>.
  120. Kim, H.-S., Jeong, G., Leem, H.J., Lee, M.A., Lee, J.-N., Woo, S.-G., and Yu, J. (2022). Positive electrode–Li metal crosstalk behavior-induced morphology change of Li deposits. *J. Mater. Chem. A* 10, 17659–17667. <https://doi.org/10.1039/D2TA03666E>.
  121. Langdon, J., and Manthiram, A. (2022). Crossover effects in lithium-metal batteries with a localized high concentration electrolyte and high-nickel cathodes. *Adv. Mater.* 34, e2205188. <https://doi.org/10.1002/adma.202205188>.
  122. Koster, D., Du, G., Battistel, A., and La Mantia, F. (2017). Dynamic impedance spectroscopy using dynamic multi-frequency analysis: a theoretical and experimental investigation. *Electrochim. Acta* 246, 553–563. <https://doi.org/10.1016/j.electacta.2017.06.060>.
  123. Wang, M., Zhang, C., Yan, S., Chen, T., Fang, H., and Yuan, X. (2021). Wide-field super-resolved Raman imaging of carbon materials. *ACS Photonics* 8, 1801–1809. <https://doi.org/10.1021/acsphotonics.1c00392>.
  124. Holler, M., Odstrcil, M., Guizar-Sicairos, M., Lebugle, M., Müller, E., Finizio, S., Tinti, G., David, C., Zusman, J., Unglaub, W., et al. (2019). Three-dimensional imaging of integrated circuits with macro- to nanoscale zoom. *Nat. Electron.* 2, 464–470. <https://doi.org/10.1038/s41928-019-0309-z>.